ANALYSIS OF SEISMIC SIGNATURES FROM GAS AND DUST BASED EXPLOSIONS AT THE LAKE LYNN EXPERIMENTAL MINE

M. M. Murphy, NIOSH, Pittsburgh, PA
A. T. Iannacchione, NIOSH, Pittsburgh, PA
E. C. Westman, Virginia Polytechnic and State Univ., Blacksburg, VA
M. C. Chapman, Virginia Polytechnic and State Univ., Blacksburg, VA

Abstract

Examination of seismic records during the time interval of the Sago Mine disaster in 2006 revealed a small amplitude signal possibly associated with an event in the mine. More needs to be understood about the seismicity from mine explosions in order to properly interpret critical seismic information. A seismic monitoring system located at NIOSH's Lake Lynn Experimental Mine has monitored experimental gas and dust based explosions and impact tests. The seismic signatures from these different events were analyzed using standard waveform analysis procedures. The magnitude of seismic energy during a gas and dust explosion was found to be more dependent on mine entry geometry and seal behavior rather than on the amount of explosive fuel present. The results suggest a large explosion that's not restricted can generate potentially the same magnitude as a small explosion that is restricted.

Introduction

Purpose of the Study

Seismic monitoring provides a powerful means for detection and evaluation of seismic events resulting from mining activity. Seismic signature characteristics such as P- and S-wave arrival times, amplitudes, signal duration and frequency content can give indication to the nature and location of the seismic source. Seismic data have been utilized in the past to analyze mining related events such as production blasts from quarries, roof falls and microseismic emissions [1-3]. However, little research has been conducted on seismicity from gas and dust explosions. The Sago Mine disaster in 2006 [4] provides an example of why the seismicity from explosions should be studied. A small amplitude signal was seen on records of regional seismic network in the time interval of the disaster [5]. The epicentral location of the signal was at the Sago Mine, however it is unclear whether the seismicity represents the explosion itself. This preliminary study will begin the process to understand the seismicity of mine explosions by studying the waveforms generated by these events at a research mine.

In order to conduct the study, a microseismic monitoring system was installed at the National Institute of Occupational Safety and Health's (NIOSH) Lake Lynn Experimental Mine (LLEM) located approximately 96 km (60 miles) southeast of Pittsburgh, PA. NIOSH's interest on the design and behavior of seals during mine explosions provided the opportunity for this research [6]. Necessary calibration measurements had to be conducted on the monitoring system in order to obtain essential variables and relationships for moment magnitude and radiated seismic energy calculations. Three gas and dust explosions at LLEM were monitored, two of which included a seal in the path of the explosive wave. The three explosions were analyzed in terms of moment magnitude and radiated seismic energy. Impact tests, in the form of dropping different sized material to the floor, were conducted to obtain physical characteristics at LLEM necessary for technical analysis. The impact tests were also analyzed in terms of moment magnitude and radiated seismic energy.

Lake Lynn Experimental Mine Overview

The Lake Lynn Experimental Mine is a full-scale mine research facility on the site of a former limestone quarry and underground mine. Research conducted at the site historically and currently has included studies on mine fires, explosions, performance of roof support products and seal design. Geologically, the mine is located in the Greenbrier limestone formation [7].

The mine layout is seen in figure 1. The west side of the facility, known as the old workings, was mined commercially in the 1960s. The dimensions of entries in the old workings are 15.2 m (50 ft) wide by 9.1 m (30 ft) high. The east side of the facility contains mine drifts which were dimensioned to match configurations found in coal mines. The dimensions of these entries are 6.1 m (20 ft) wide by 2.0 m (6.5 ft) high. A-, B-, C- and E-Drifts are approximately 480 – 495 m (1,575 – 1,630 ft) long. E-Drift is 155 m (510 ft) long. The size of the pillars in the entry section is 24 x 12 m (80 x 40 ft).

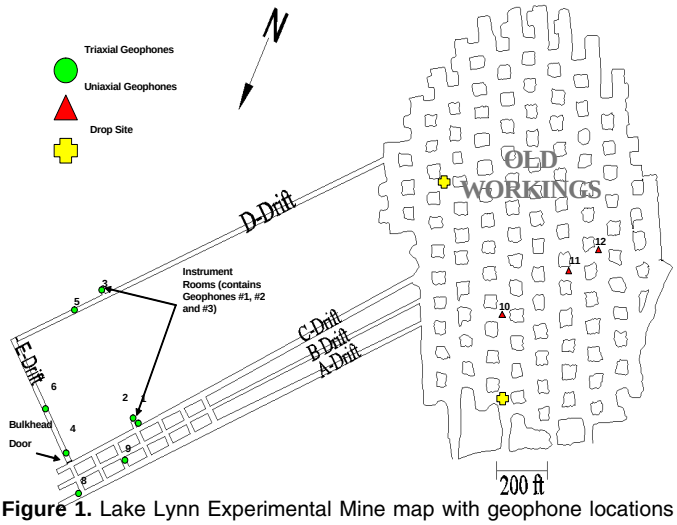

Figure 1. Lake Lynn Experimental Mine map with geophone locations indicated. Geophone #7 was used as a test geophone and is not included in geophone monitoring array. Triaxial geophones were installed in the drift area while uniaxial geophones were installed in the old workings. The drop sites used for the impact studies are located in the old workings.

A bulkhead door is shown in figure 1 at the intersection of E-Drift and C-Drift. This 70-ton door, constructed in place with steel framework and reinforced concrete, was closed during the explosion tests. Instrument rooms in the mine are located approximately three quarters of the way down C- and D-drifts. These rooms are protected from the entry via submarine-type doors. The instrument rooms provide a pre-wired network so the digitizers can be connected to a central PC outside of the mine.

Microseismic Monitoring System Components

The basic components of the microseismic monitoring system include the geophone, digitizer, modem rack, serial hub and data acquisition computer, as outlined in figure 2. The triaxial geophones used are the Sercel L-28[1], which have a natural frequency of 4.5 Hz. Two different types of digitizers, manufactured by ISS International are used: Microseismic (MS) boxes and Quake Seismometer (QS) boxes. Both types of digitizers have a sampling rate of 2,000 samples per second and contain six channels for input. The modem rack allows up to sixteen digitizers online with the system via DB-9 connector ports. The serial hub takes the sixteen ports from the modem rack and converts them into a single 100/10 LAN cable connected to the data acquisition computer. The digitizers send data to the computer when the geophones are triggered based upon pre-set threshold values.

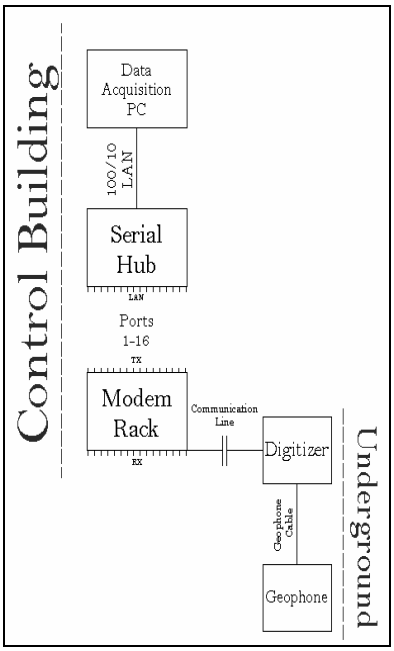

Figure 2. Components of the microseismic monitoring system.

Experimental Procedure

Digitizer Calibration

Before the seismically recorded magnitude and energy can be calculated for events monitored in this study, the number of digital counts for a one volt input signal as a function of frequency needed to be determined. The phase response of the digitizers is not needed. The number of counts per volt for each digitizer was measured by using a waveform generator to input a sinusoidal wave of a specific frequency. The response to each calibration frequency, between 50-1,000 Hz at 50 Hz intervals, was digitized and plotted in figure 3. The QS box has a constant response at both low and high frequencies. The sudden change in high frequency response of the curve is due to the anti-alias filter near the Nyquist frequency of 1,000 Hz.

[1]Mention of specific products or manufacturers does not imply endorsement by the National Institute of Occupational Safety and Health.

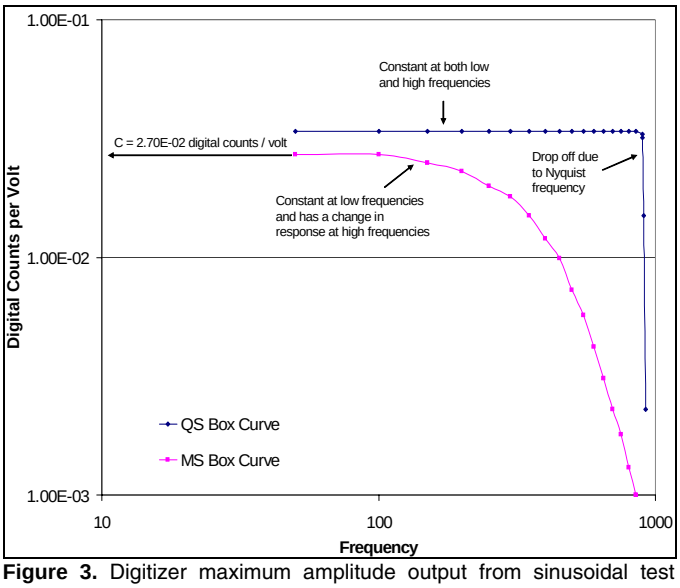

Figure 3. Digitizer maximum amplitude output from sinusoidal test calibration. The measured points are represented by the dots in each of the curves.

The results show that the MS box response is constant at low frequencies up to approximately 100 Hz. The loss in amplitude at higher frequencies is due to a low-pass filter built into the MS box. The amplitude response of the low-pass filter G(ω) was derived.

$$G(\omega) = \frac{1}{1+\left(\frac{\omega}{\omega_c}\right)^3} \qquad (1)$$

where $\Omega = 2\pi f$, f = frequency in Hz,
$\omega_c = 2\pi f_{corner}$, f_{corner} = frequency in Hz.

The digitizer constant, needed to calculate the system amplitude response to both ground displacement and velocity, was also determined from the calibration. The constant, C, is 0.027 counts/volt for the MS box and 0.034 counts/volt for the QS box.

Determination of System Amplitude Response to Ground Displacement and Velocity

The system amplitude responses to ground displacement and velocity are needed for moment magnitude and radiated seismic energy calculations. System amplitude responses to ground displacement and velocity can be derived using a single degree of freedom damped spring-mass system model [8], the Sercel geophone product sheet [9] and the results of the digitizer calibration test described previously. The system amplitude response to ground displacement, D(ω), is shown below and plotted in figure 4.

$$D(\omega) = \left(\frac{EC\omega^3 \left(\frac{R_s}{R_t}\right)}{\sqrt{\left(\omega_o^2 - \omega^2\right)^2 + \left(2h\omega_o\omega\right)^2}} \right) G(\omega) \qquad (2)$$

where: E = geophone electrodynamic constant (volts/m/s),
C = digitizer constant, determined from sinusoidal input test (digital counts/volt),
$\Omega = 2\pi f$ (frequency in Hz),
R_s = shunt resistance for a given damping (ohms),
R_t = total circuit damping (ohms),
$\omega_o = 2\pi f_{natural}$ (natural frequency in Hz), and
H = geophone damping.

Figure 4 shows that above the geophone natural frequency of 4.5 Hz, the slope of the response line is equal to one. Below the natural frequency of the geophone, the slope is equal to three. This response behavior is expected for an amplitude response to ground displacement using a velocity transducer [8]. At frequencies above 100 Hz for the MS box, the response changes because of the low pass filter. The system amplitude response to ground velocity, V(ω), is shown below and plotted in figure 5.

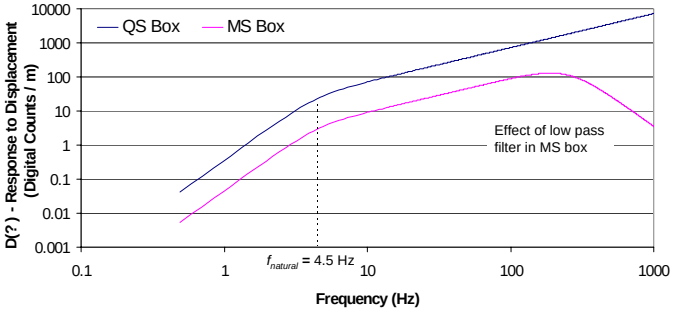

Figure 4. System amplitude response to displacement.

$$V(\omega) = \left(\frac{EC\omega^2 \left(\frac{R_s}{R_t} \right)}{\sqrt{\left(\omega_o^2 - \omega^2\right)^2 + \left(2h\omega_o\omega\right)^2}} \right) G(\omega) \qquad (3)$$

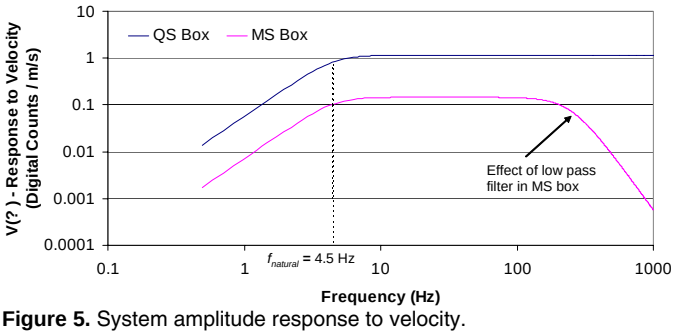

Figure 5. System amplitude response to velocity.

Geophone Location and Placement

A geophone location map with identification numbers can be seen in figure 1. Triaxial geophones are located in the drift area and uniaxial geophones are located in the old workings. The uniaxial geophones were oriented vertically and were mounted on the ground. All triaxial geophones were mounted on the excavation surface about 3 m (10 ft) from the floor, except for Geophone #1 which was on the floor and Geophone #4 located on a concrete block attached to the roof. The horizontal components of the triaxial geophones were similarly oriented with components parallel and perpendicular of A-D drifts, approximately 50 degrees east of true north. A metal bar with holes on each end holds the geophone in place while pieces of all-thread rods are bored into the roof to tighten the bar and secure the geophone. The horizontal components were leveled and the vertical components were checked for verticality. No epoxy was used to mount the geophones.

Explosion Tests

Natural gas (~98% methane) is injected into a 14 m (47 ft) long ignition chamber at the face of C-Drift, and an electric fan with an explosion-proof motor housing mixes the natural gas with the air to result in an approximately 9.5% methane-air concentration. The flammable natural gas-air volume was ignited using a triple-point ignition source. This ignition source consists of three sets of two 100-J electric matches that are equally spaced at midheight across the closed end and ignited at the same time. Five barrels filled with water, located near the outby end of the ignition chamber, act as turbulence generators to achieve a projected pressure pulse. To increase the explosion pressure, either the ignition chamber is lengthened or pulverized coal dust is suspended on shelves from the mine roof starting just outside of the ignition chamber. Pressure transducers at the location of the heading seal (or the seal construction across C-drift approximately 98 m (320 ft) from the face) were used to measure the peak pressure of the explosion. When the explosion pulse reaches the seal across C-drift, it is reflected, and the resulting total reflected pressure can be about twice the incoming pressure pulse value. The three explosion tests conducted at Lake Lynn Experimental Mine were named LLEM Shots #507 through #509. Figure 6 is a schematic of the initial amount of explosive fuel, seal locations and measurement of explosion pulse pressure for each test.

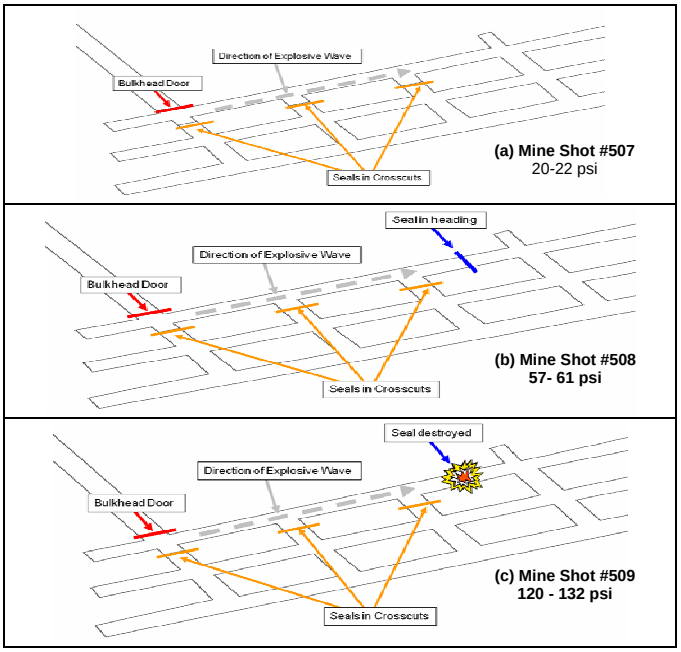

Figure 6. Setup of the three explosion tests during the experiment. The pressure value is the peak generated pressure of the explosive wave measured at the location of the seal in the heading.

Shot #507 was conducted on November 1, 2006. For this experiment, there was no seal located across C-Drift entry. The test was designed to generate 20-22 psi transverse pressure against the crosscut seals. The initial amount of explosive fuel was 18.7 m^3 (661 ft^3) of natural gas and 3.6 kg (8 lbs) of coal dust. Shot #508 was conducted on April 10, 2007 and Shot #509 was conducted on April 12, 2007. The purpose of these shots was to test a heading seal across C-Drift. The same seal was tested during both shots. The pressure against the heading seal was approximately 57-61 psi for Shot #508 and 120-132 psi for Shot #509. The pressure transducer was located near the center of the seal in a horizontal position facing the oncoming explosion. The initial amount of explosive fuel was 18.7 m^3 (661 ft^3) of natural gas and 3.6 kg (8 lbs) of coal dust for Shot #508. For Shot #509, the amount of initial explosive fuel was 35.8 m^3 (1,265 ft^3) of natural gas and 14.5 kg (32 lbs) of coal dust. The seal failed during Shot #509. For Shot #507, the uniaxial geophones in the old workings were not part of the monitoring system. For Shot #508, Geophones #1 and #2 in C-Drift were unable to monitor.

Drop Tests

Drop tests were conducted to help obtain P- and S-wave velocities necessary for analysis. Two locations inside of the mine were chosen for drop sites (figure 1). At both sites the limestone floor was exposed and was free of debris. Rocks of various sizes were dropped from a height of 3.2 m (10.6 ft). Also dropped during the

experiment were a 725 kg (1,600 lb) concrete block and a 1,429 kg (3,150 lb) block of steel. Seven drop tests are included for this study. During the drop tests, only Geophones #10, #11 and #12 close to the drop sites in the old workings registered the events.

Data Analysis Procedure

Data collected during the experiment were analyzed in terms of static seismic moment [10], moment magnitude [11] and radiated seismic energy [12].

Determination of Moment Magnitude

The static seismic moment, M_o, is derived from the Fourier displacement amplitude spectrum.

$$M_o = \frac{4\pi\rho R|\Omega_o|c^3}{F_c} \qquad (4)$$

where ρ = density of the rock at the source (kg/m^3),
R = distance from source to receiver (m),
Ω_o = low frequency spectral plateau seen in the Fourier displacement amplitude spectrum (m/Hz),
C = P- or S-wave velocity (m/s), and
F_c = P- or S-wave radiation pattern coefficient.

For the static seismic moment calculations, it is assumed the events produce an isotropic wave radiation pattern. The static seismic moment is expressed in units of N•m. The low frequency spectral plateau, Ω_o, can be found from the Fourier amplitude spectrum of ground displacement. The raw signal collected by the geophone is in units of digital counts. The Fourier amplitude spectrum of that raw signal, in units of digital counts per Hz, can be represented by S( ). Thus, the Fourier amplitude spectrum of ground displacement, in units of meters per Hz, is determined from the Fourier amplitude spectrum from the raw signal and the system amplitude response to ground displacement described earlier.

$$D(f) = \frac{S(\omega)}{D(\omega)} \qquad (5)$$

An example of the Fourier amplitude spectrum of ground displacement can be seen in figure 7. The noise curve represents the pre-signal noise. A dotted line shows the overall trend for the signal displacement curve. The low frequency spectral plateau is where the curve flattens out above low frequencies, as indicated in figure 7. Although three low frequency asymptotes were found for each triaxial geophone (one per component), only one value of moment magnitude is reported, based on the arithmetic mean of the three asymptotes for the three components. The moment magnitude, *M,* is determined from the static seismic moment by the relationship:

$$M = \frac{2}{3}\log(M_o) - 6 \qquad (6)$$

Determination of Radiated Seismic Energy

The radiated seismic energy, E_s, is expressed in units of joules. The radiated seismic energy for an isotropic source is given by:

$$E_s = 4\pi\rho c R^2 (I_1 + I_2 + I_3) \qquad (7)$$

where ρ = density of the rock at the source (kg/m^3),
R = distance from source to receiver (m),
c = P- or S-wave velocity (m/s), and
I = integral of squared velocity for a geophone orientation (m^2/s^2/Hz).

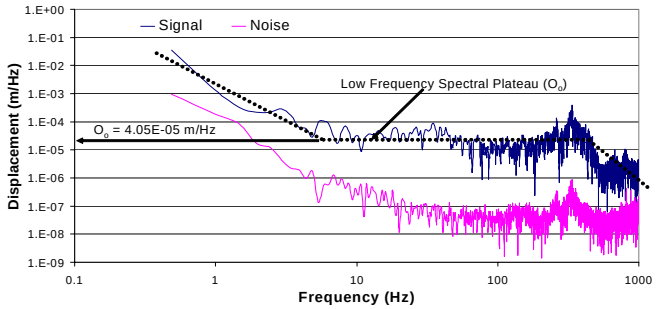

Figure 7. Example of the Fourier amplitude spectrum of ground displacement. The noise curve is the amplitude spectrum of the background noise and the signal curve is the amplitude spectrum of the event being characterized.

The integral of squared velocity, I, is determined from the Fourier amplitude spectrum of ground velocity. The Fourier amplitude spectrum of ground velocity, in units of m/s per Hz, is determined from the Fourier amplitude spectrum of the raw signal and the system amplitude response to ground velocity.

$$V(f) = \frac{S(\omega)}{V(\omega)} \qquad (8)$$

An example of the Fourier spectrum of ground velocity can be seen in figure 8. The integral of squared velocity is the area between the signal and noise curves where they separate and merge together between two frequency values. The two curves showed similar trends up to 7 Hz, so this would be the frequency where the energy area begins. Where the two curves merged back together is the frequency where the energy area ends. For the uniaxial geophones, equal amplitude is assumed on all three components. The single component estimate for I is multiplied by a factor of three.

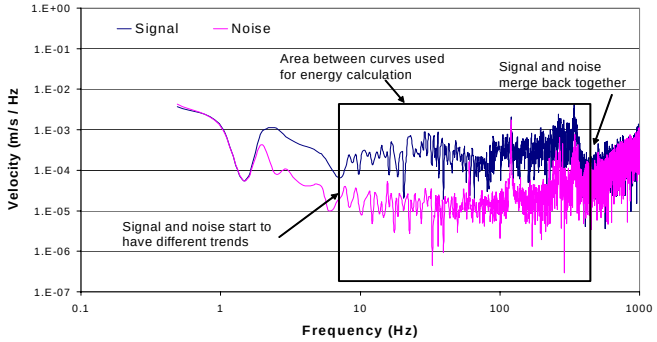

Figure 8. Example of the Fourier amplitude spectrum of ground velocity. The noise curve is the amplitude spectrum of the background noise and the signal curve is the amplitude spectrum of the event being characterized. Energy below the natural frequency of the geophone was included in some cases because the amplitude response formulas were derived for all frequencies.

Determination of P- and S-Wave Velocity

The results from the seven drop tests can be seen in Table 1. An earlier study showed that P- and S-waves are generated during drop tests [1]. The P- and S-wave arrival time difference was minimal for each drop, so the S-wave had to be determined from the P-wave arrival time. The S-wave velocity was calculated by dividing the P-wave velocity by $\sqrt{3}$. The P- and S- wave velocities used for technical analysis were 4,511 m/s (14,800 ft/sec) and 2,604 m/s (8,545 ft/sec), respectively. These values are in the same velocity range as another limestone formation in Pennsylvania [1].

Table 1. P- and S-wave velocities (m/s) of the drop tests conducted for the study.

Test	P-Wave	S-Wave
1	3,677	2,123
2	4,760	2,748
3	4,252	2,455
4	4,511	2,604
5	4,111	2,373
6	6,380	3,683
7	4,577	2,643
Mean	4,610	2,661
Standard deviation	8.58	495
Median	4,511	2,6048

Discussion of Results

Discussion of Explosion Tests

While it is usually advantageous to have instruments close to the events, in some cases it can present a problem. At close range, a variety of phases such as acoustic waves and seismic surface waves may be present in the waveforms, in addition to the direct seismic P and S waves of interest. The moment magnitude and radiated seismic energy equations as defined here should be estimated from the direct P or S wave arrivals. Thus, values for magnitude and energy would be misrepresented if the analysis of the waveform included more than just a direct body wave arrival.

It is believed that recordings from the closest instruments, Geophones #1, #2, #4, #6, #8 and #9 recorded multiple phase arrivals. In order to investigate this theory, the waveform from Geophones #10 and #12 for Shot #509 was analyzed. There appears to be two distinct phases in this waveform, as shown in figure 9. The two phases are believed to be the seismic energy due to the explosion and the acoustic air blast, respectively. Knowing the P-wave velocity determined from the drop tests and difference in arrival times between the two phase arrivals, a velocity can be found for the second arrival. The velocity of the second phase arrival was found to be approximately 320 m/s (1,050 ft/sec), consistent with the speed of sound of air. The latter is a function of temperature, which for the mine (at 55° F) would be approximately 340 m/s (1,100 ft/sec), sufficiently close to validate the second phase as the acoustic air blast. Much closer to the ignition of the explosion in C-Drift, the waveforms can be expected to represent a combination of the acoustic and seismic energy; however, the clear distinction as shown in figure 9 won't be seen.

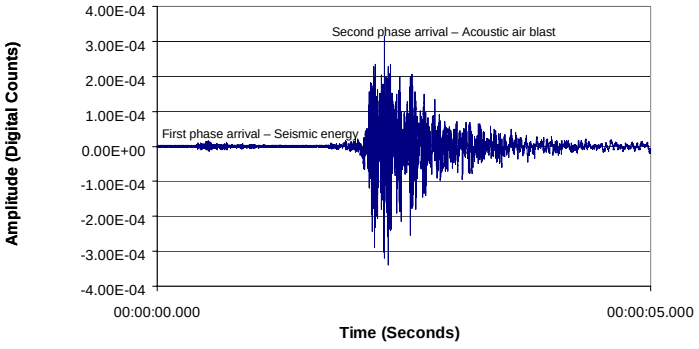

Figure 9 . Geophone #10 waveform from Shot #509.

The two geophones in D-Drift, Geophones #3 and #5, are assumed to record pure seismic energy, because they were not in the path of the air blast and were relatively far away. The magnitudes and energies, as calculated from geophones in D-Drift, are shown in figure 10 and 11, respectively. The magnitude and energy values were calculated with the assumption that the explosive source is in the far field. Based upon these two charts, it can be seen that Shot #508 has a higher magnitude and energy when compared to Shot #507. As stated previously, these two tests contained the same initial amount of explosive fuel and the only difference was Shot #508 contained a heading seal (as seen in figure 6). The results show that the addition of a seal in the path of an explosive wave generates more seismic energy. The additional seismic energy can be a result of the seal flexing and causing the roof, floor and rib to vibrate. Between these two shots it can be concluded that the magnitude of seismic energy is more dependant on mine entry geometry and seal behavior than on the amount of fuel present. Therefore, the results suggest a large explosion that's not restricted can generate potentially the same magnitude as a small explosion that is restricted. For Shot #509, the magnitude and energy is higher than the previous two shots. However, this shot started with a higher amount of initial explosive fuel and the seal fails, which causes impacts of seal material debris against the rib and floor. The additional seismic energy recorded for this explosion is likely due to these factors.

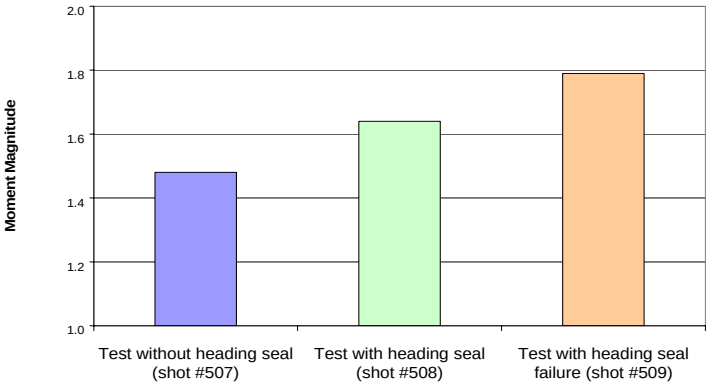

Figure 10. Moment magnitude values of the three mine shots. Note that Shots #507 and #508 had the same initial explosive fuel

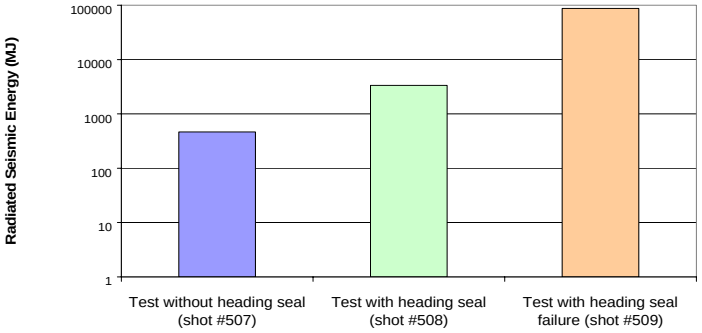

Figure 11. Radiated seismic energy values of the three mine shots.

Discussion of Drop Tests

A plot of magnitude versus mass of material and energy versus mass of material for the drop tests can be seen in figures 12 and 13, respectively. If a regression line is fit through the whole dataset in figure 11, the value of R^2, the square of the sample correlation coefficient, is 0.39 which is very poor. Looking at figure 12, the regression line through the whole dataset has an R^2 value of 0.78. The data scatter and poor fit appear to be related to how the material impacted the ground. When the concrete and steel blocks hit the limestone floor, the amount of surface area that made contact was very high. In contrast, most of the limestone blocks were bulky and irregular in shape. When they hit the floor, little of the limestone surface made direct contact and a lot of energy was consumed by breaking the limestone rock into multiple pieces. Thus, the amount of seismic energy effectively transferred into the ground may be highly variable. Based on observations during the tests, the concrete block, the steel block and the 4- and 12-ton limestone rocks hit the floor with maximum surface contact. Regression lines through those data points are shown in figures 12 and 13, with R^2 values of 0.86 and 0.99,

respectively. These high R^2 values suggest that the degree of surface contact upon impact is an important contributor to seismic efficiency and high magnitude estimates.

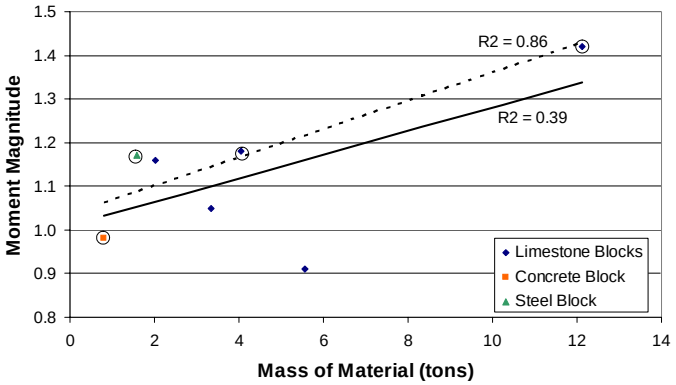

Figure 12. Moment magnitude versus mass of material dropped from a height of 3.2 m (10.6 ft). The solid regression line is for all the data points. The dashed regression line is for the circled four data points, which indicate the dropped material that impacted the floor with maximum surface contact.

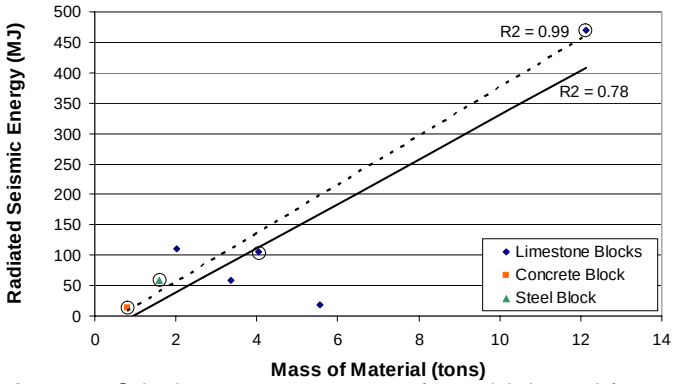

Figure 13. Seismic energy versus mass of material dropped from a height of 3.2 m (10.6 ft). The solid line is for all the data points. The dashed regression line is for the circled four data points, which indicate the dropped material that impacted the floor with maximum surface contact.

Conclusions

The following conclusions are based upon the measurements of moment magnitude and radiated seismic energy calculations from the three mine shots and the seven drop tests:

- During the explosion tests for this study, some of the geophones were believed to have captured a variety of waveform phases, such as acoustic waves and seismic surface waves. With these phases included in the waveform, the measured values for moment magnitudes and radiated are inaccurate because the recorded waveforms are not from a pure seismic source.
- The unwanted phases would not ordinarily be present in the waveforms from an explosive event if the geophones were further away or in a borehole. However, in the case of this study, the geophone array and the inability at the time to put geophones in a borehole allowed these phases to be recorded.
- Geophones #3 and #5 were assumed to capture only seismic energy because these geophones were not in the path of the explosive wave and relatively far away.
- The magnitude of seismic energy during a gas and dust explosion was found to be more dependent on mine entry geometry and seal behavior than on the amount of explosive fuel present. The results suggest a large explosion that's not restricted can generate potentially the same magnitude as a small explosion that is restricted.

Disclaimer

The findings and conclusions in this report have not been formally disseminated by the National Institute for Occupational Safety and Health and should not be construed to represent any agency determination or policy.

Future Research

An analytical method is being developed to separate the unwanted phases from the waveforms. By separating out these phases, more data is provided for the explosive test results which will provide additional understanding of the seismic signatures. The second phase arrival, as seen in figure 9, was shown to be the acoustic air blast. This provides a starting point to successfully remove that phase from the waveforms. A similar method is being developed to separate out the seal failure and subsequent impacts from the waveforms captured during Shot #509, to see how much the additional explosive fuel had an effect on the seismic energy. More explosive tests at the Lake Lynn Laboratory Experimental Mine are planned for the future and will be monitored.

References

1. Iannacchione, A. T., L. M. Burke, and M. C. Chapman (2005), "Characterizing Roof Fall Signatures From Underground Mines," in the *Proceedings of the 6th International Symposium on Rockburst and Seismicity in Mines,* Perth, Australia, March 9-11, Australian Centre for Geomechanics. p. 619-629.
2. Iannacchione, A. T., G. S. Esterhuizen, T. S. Bajpayee, P. L. Swanson and M. C. Chapman (2005), "Characteristics of Mining-Induced Seismicity Associated with Roof Falls and Roof Caving Events," in the *Proceedings of the 40th U.S. Rock Mechanics Symposium,* Anchorage, AK.
3. Swanson, P., B. Kenner, and T. Krahenbuhl (2002), "Seismic Event Data Acquisition and Processing: Distribution and Coordination Across PC-Based Networks, in Application of Computers and Operations Research in the Mineral Industry," in the *Proceedings of the 30th International Symposium*, S. Bandopadhyay Ed., Society of Mineral Metallurgy, and Exploration.
4. Mining Health and Safety Administration (2007), "Report of Investigation - Fatal Underground Coal Mine Explosion - January 2, 2006 - Sago Mine, Wolf Run Mining Company - Tallmansville, Upshur County, West Virginia," ID No. 46-08791,. http://www.msha.gov/Fatals/2006/Sago/sagoreport.asp
5. Chapman, M. C. (2006), "Appendix CC - Results from Analysis of Seismic Data for the January 2, 2006, event near Sago, WV," Virginia Polytechnic Institute and State University: Blacksburg, VA.

   http://www.msha.gov/Fatals/2006/Sago/sagoreport.asp
6. Zipf, R. K., M. J. Sapko, and J. F. Brune (2007), "Explosion Pressure Design Criteria for New Seals in U.S. Coal Mines," Publication No. 2007-144, Department of Health and Human Services, Public Health Service, Centers for Disease Control and Prevention, NIOSH, DHHS: Pittsburgh, PA.
7. Triebsch, G. and M. J. Sapko (1990), "Lake Lynn Laboratory: A State-of-the-Art Mining Research Facility," in the *Proceedings of the International Symposium on Unique Underground Structures*, *2*:75-1 - 75-21.
8. Aki, K. and P.G. Richards (2002), "*Quantitative Seismology*," Second Edition, ed. J. Ellis., Sausalto, CA: University Science Books.

9. Sercel (2005), "L-28 Digital Grade Geophone," ftp://ftp.sercel.com/pdf/brochures/GeophonesHydrophones.pdf.
10. Aki, K. (1968), "Seismic Displacements near a Fault", *Journal of Geophysical Research*, *73*(16):5359-5376.
11. Hanks, T. and H. Kanamori (1979), "A Moment Magnitude Scale," *Journal of Geophysical Research*,. *84*(B5):2348-2350.
12. Boatwright, J. and J. B. Fletcher (1984), "The Partition of Radiated Seismic Energy Between P and S Waves," *Bulletin of the Seismological Society of America*, *74*:361-376.